# 1

# Magnetoelectric Effect of Functional Materials: Theoretical Analysis, Modeling, and Experiment

*Jia-Wei Zhang*[1,2], *Hong-Yan Guo*[1], *Xiao Chen*[1], *and Rui-Tong Liu*[3]

[1] *Northeast Electric Power University, School of Electrical Engineering,169 Changchun Road, Jilin 132013, China*
[2] *Harbin University of Science and Technology, Key Laboratory of Engineering Dielectric and its Application of Ministry of Education, Harbin, China*
[3] *State Grid Liaoning Province Power Company Limited Power Research Institute, Shenyang 110181, China*



## 1.1 Introduction of Magnetoelectric Effect

Magnetoelectric (ME) effect is defined as an induced dielectric polarization under an applied magnetic field and/or an induced magnetization under an external electric field [1]. Materials with ME properties are called magnetoelectric materials (MMs). There are single- and multiphase MMs. Single-phase MMs contain only one type of structure. Little research has been done on single-phase MMs because the intrinsic ME coupling in single-phase compounds is generally quite weak, especially at room temperature. The ME effect in multiphase composite materials is the product of ferromagnetic magnetostriction and ferroelectric piezoelectricity [2].

### 1.1.1 Single-Phase Magnetoelectric Materials

Single-phase materials possessing both antiferromagnetic and ferroelectric constituents in the same phase are the first discovered ME materials. In 1894, Pierre Curie predicted the possibility of an intrinsic ME effect in some single-phase materials. Although the terminology "magnetoelectric effect" was defined by Debye in 1926, it remained a speculation until 1960 when the first real MM $Cr_2O_3$ was discovered [3]. In 1969, Homreich discovered some candidates of MMs based on the magnetic point group, including $Fe_2TeO_6$, $Cr_2TeO_6$, $FeCrWO_6$, $Cr_2WO_6$, $Ca_2FeAlO_5$, and $FeNaO_2$. In 1970, $BiFeO_3$ was found to be unique among various ME multiferroics because of its exceptionally high antiferromagnetic and ferroelectric transition temperatures well above room temperature [4]. An important breakthrough in 2003 was the discovery of large room-temperature ferroelectric polarization in coexistence with magnetization in $BiFeO_3$ thin films, which presents a theoretical investigation on $BiFeO_3$ bulks, films, and heterostructures.

*Magnetoelectric Polymer-Based Composites: Fundamentals and Applications*, First Edition.
Edited by Senentxu Lanceros-Méndez and Pedro Martins.

### 1.1.2 Multiphase Materials

In the past century, to overcome the drawbacks of weak ME effect in single-phase materials, ME materials have evolved from single-phase compounds to multiphase materials. Multiphase materials are usually prepared by combining ferromagnetic and ferroelectric phases in the bulk and laminated forms.

In 1948, Tellegen failed to synthesize bulk composites with extrinsic ME effect by combining two different types of macroscopic particle composites with magnetic and electric dipole moments as the beginning of the investigation. In the early 1990s, bulk composites of ferrites and $BaTiO_3$ or Pb(Zr, Ti)$O_3$ (PZT) had been prepared by Newnham's group and Russian scientists through a conventional sintering process. In 2001, Patankar *et al.* performed extended experiments on several doped ferrite/titanate bulk composites such as $CuFe_{1.8}Cr_{0.2}O_4/Ba_{0.8}Pb_{0.2}TiO_3$. Recently, experiments on many doped titanate/ferrite composites were reported. The piezoelectric constituents include $Bi_4Ti_3O_{12}$, polyvinylidene fluoride (PVDF), $PbMg_{1/3}V_{2/3}O_3$, and $PbX_{1/3}Nb_{2/3}O_3$-$PbTiO_3$ (X = Mg, Zn), and the alternative magnetostrictive constituents include $LiFe_5O_8$, yttrium iron garnet (YIG), and Permendur [5].

Laminated composites are typically made of magnetostrictive material layers bonded with piezoelectric material layers with different arrangements of the magnetization and polarization directions. Figure 1.1 shows an example of the epoxy-bonded-type three-phase laminated composites constructed by sandwiching a thickness-polarized PZT plate between two length-magnetized epoxy-bonded Terfenol-D particulate composite plates [7].

Recently, the direct-coupling Lorentz force effect in the metallic phase with the piezoelectric effect in the piezoelectric phase induced by an extrinsic "dc" ME effect was observed in metallic/piezoelectric heterostructures. Guiffard *et al.* developed an ME current sensor with ME coupling in a simple piezoelectric unimorph bender induced by the eddy currents within the silver electrodes of the piezoelectric ceramic PZT subjected to ac magnetic flux [8]. Therefore, the MMs without the magnetic phase can be used in ME current sensors.

## 1.2 Applications of Magnetoelectric Effect

So far bulk composites, laminated composites, and metallic/piezoelectric heterostructures exhibit practically useful ME effect above room temperature.

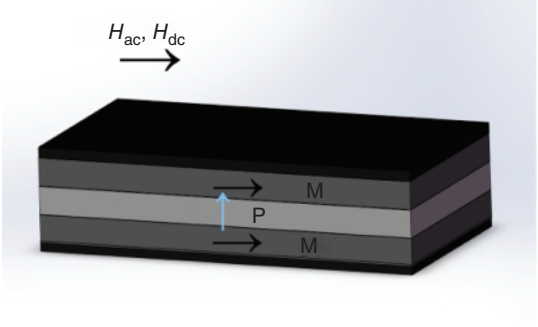


**Figure 1.1** Schematic of proposed laminated composites configuration of magnetostrictive and piezoelectric materials [6].

Nowadays, there are some main promising device applications, including ME sensors, ME transducers, ME microwave devices, and so on.

### 1.2.1 Magnetoelectric Sensors

In the work of Leung *et al.*, a high-sensitive magnetoelectric sensor was obtained using ME composites by increasing the corresponding ME voltage coefficient of 27 mV $Oe^{-1}$ during measurement [9].

The working principle of the sensor was as follows: when an ac vortex magnetic field was induced along the length of the electric cable by an ac electric current in the cable in accordance with Ampère's law, the sensor transduced the ac vortex magnetic field to an ac electric voltage based on the giant ME effect.

### 1.2.2 Magnetoelectric Transducer

Today, the magnetoelectric transducer has become a hot research topic, partly because the energy harvest from the environment has been considered to be a significant investigation by researchers. There are four main types of vibration energy harvesters (VEHs), namely electrostatic, piezoelectric, ME, and electromagnetic (EM) [10].

The VEH that consisted of a ME/EM composite transducer, a cantilever beam, and magnetic circuits was reported by Qiu and coworkers. The schematic diagram of the proposed ME/EM composite VEH is shown in Figure 1.2a. The ME/EM composite transducer was placed at the tip of the cantilever beam and could act as masses, which lowered the natural frequency of the cantilever beam and scavenged lower frequency vibration energy from environments more effectively. The schematic diagram of the ME/EM composite transducer is shown in Figure 1.2b. The transducer was made up of a coil and a three-phase laminate, which is composed of two Terfenol-D layers and a piezoelectric layer.

The working principle of the ME/EM composite transducer is as follows: based on Faraday's law of electromagnet induction, when the composite transducers undergo alterations of magnetic flux gradient generated by a vibration source,

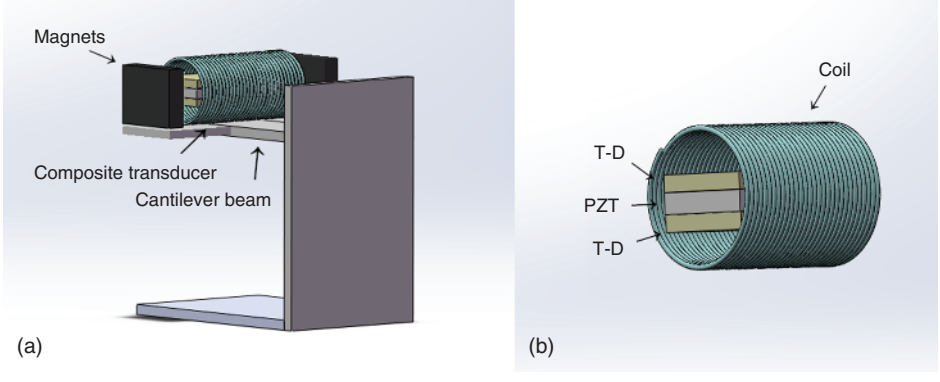


**Figure 1.2** Schematic diagrams of (a) the proposed ME/EM composite VEH and (b) the ME/EM composite transducer [10].

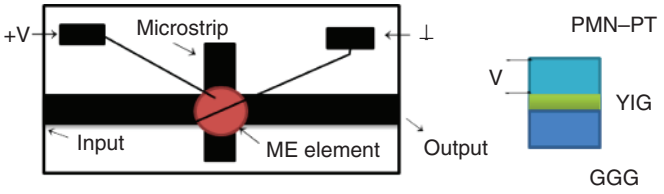


**Figure 1.3** Design of microstrip ME attenuator and ME resonator [13]. Tatarenko and Bichurin 2012 https://www.hindawi.com/journals/acmp/2012/286562/abs/. Used under CC BY 3.0 license.

the coil would induce an electromotive force due to the relative motion between the coil and the magnetic circuit. Meanwhile, based on the ME effect, the stresses induced by Terfenol-D layers would transmit to the piezoelectric layer, and finally the electrical power is generated.

### 1.2.3 Magnetoelectric Microwave Devices

Magnetoelectric microwave devices are the devices that can be tuned by magnetostatic field and electrostatic field when the devices are applied with composited MMs. Because of the advantages of low power consumption, low noise, and high-quality factor, the ME microwave devices have great potential in mobile communication system, electronic warfare systems, active phased-array radar under the national defense platform, and so on [11].

The attenuator with a microstrip transmission line on dielectric substrate and ME resonator was reported by Tatarenko *et al.* With the influence of an external electrical field, the ME effect shifted the line of FMR (ferromagnetic resonance), which is a powerful tool for the studies of microwave ME interaction in ferrite-piezoelectric structures [12].

As shown in Figure 1.3, the sample of layered structure consisted of the magnetic part with the YIG thin film placed on the GGG film and the piezoelectric part with the thin PMN–PT plate. Based on resonance ME effect phenomena, when applying the control voltage to electrodes of the ME resonator, a shift of FMR line would occur due to the resonance ME effect, and hence electrical tuning is realized.

## 1.3 Magnetoelectric Effect of Piezoelectric Ceramic

Previous reports of magnetoelectric materials with magnetostrictive/piezoelectric magnetoelectric laminates have been discussed by many researchers. However, it requires ac current supply on the electrically conductive Terfenol-D strips. Recently, the ME effect in the piezoelectric beam based on torque moment, which is generated from Lorentz force on the electrodes without magnetic phase in the sample and also without applying power source on the piezoelectric beam, has been reported by Zhang *et al.*

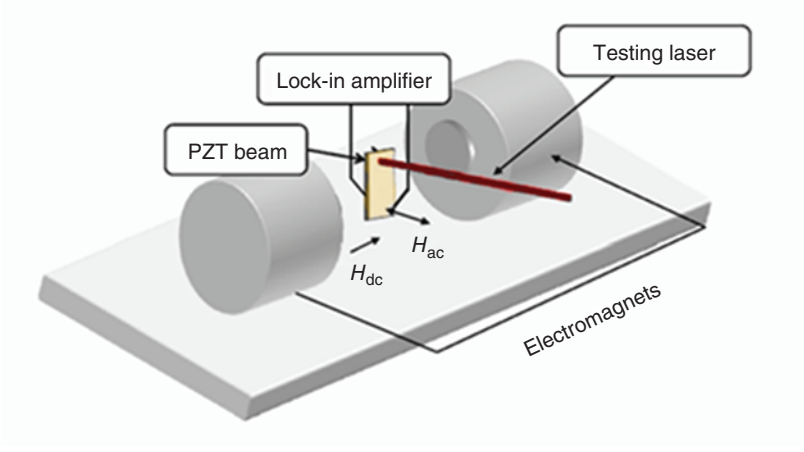


**Figure 1.4** Schematic drawing of the experimental system of ME actuator and its torsion velocity measurement [14].

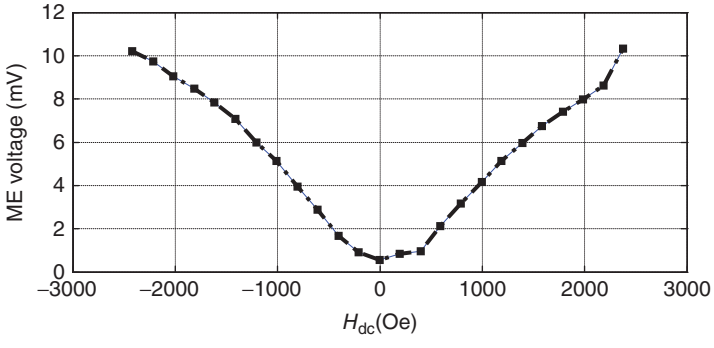


**Figure 1.5** Torsion velocity of PZT beam versus the same dc magnetic field.

As shown in Figure 1.4, the measuring system was composed of a PZT beam and an electric wire, which induced the ac magnetic field that penetrated into the surface of the PZT beam. When the metal electrodes of the PZT beam were subjected to ac magnetic fields with suitable directions, frequency, and amplitude, the moment appearing in the sample surface would apply the Lorentz torque force, and thus the mangetoelectric voltage was generated. The lock-in amplifier was used for measuring the induced ME voltage at room temperature. The torsion velocity measurement was performed on the sample by using a laser vibrometer system composed of laser controller and a laser sensor head to prove that the apparent ME effect was a coupled magnetic and electrical phase through mechanical interaction. Figures 1.5 and 1.6 show a linear ME response that the voltage and torsion velocity of PZT beam are proportional to $H_{dc}$ when 1 Oe ac magnetic field is applied with a constant frequency of 480 Hz (resonance frequency of piezoelectric beam).

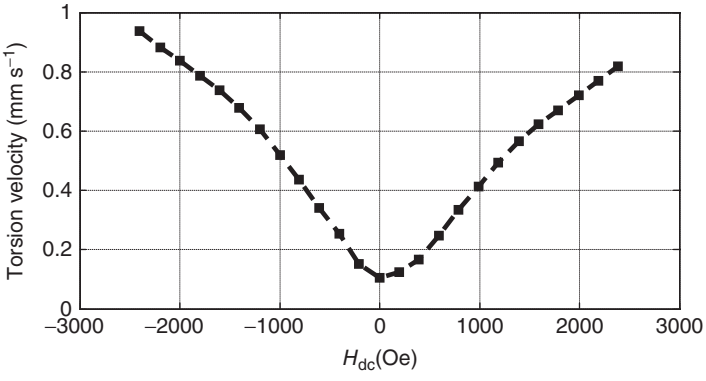


**Figure 1.6** Torsion velocity of PZT beam versus the same dc magnetic field.

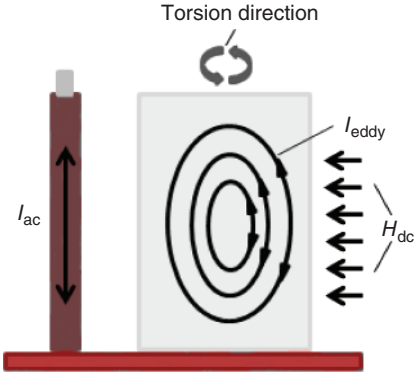


**Figure 1.7** Schematic diagram of the rectangular shape piezoelectric beam subjected to ac and dc magnetic fields.

In this experiment, the result of the linear ME response can be explained as that the magnitude of dc magnetic field from 0 to ±2400 Oe was proportional to the magnitude of the moment on the metal layer due to enhanced eddy current. From the aforementioned phenomenon, the ME response would be enhanced by increasing the torsion deformation, which is induced by the moment. Therefore, the generalized ME response without magnetic phase and also without applying power source in the measuring system was observed.

In addition, in order to explore the ME effect in piezoelectric ceramic and the application of ME sensor, the investigation with magnetic actuator has also been developed by Zhang *et al.*

As shown in Figure 1.7, the measuring system for investigating the ME response and torsion deformation of the beam was composed of a piezoelectric beam, an electromagnet, and an ac conducting wire, which induced the ac magnetic flux that penetrated into the metal part of the sample to generate eddy current. Due to the coupling of the piezoelectric layer and Lorentz force from the eddy current, piezoelectric bender's torsion deformation could be induced by Lorentz force, and thus piezoelectric voltage appeared on the sample [15].

As shown in Figures 1.8 and 1.9, the experimental results of PZT bender's voltage and the velocity and an approximate linear relation of ME voltage and torsion

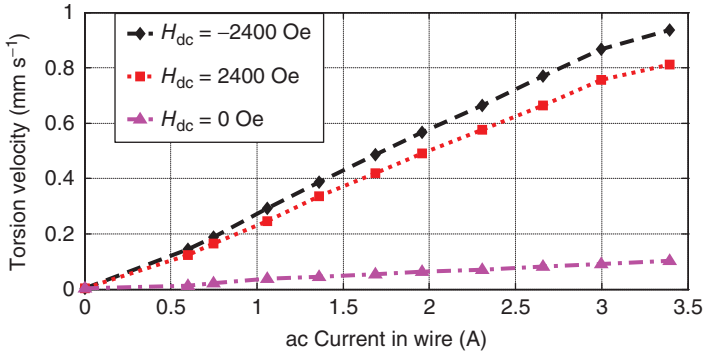


**Figure 1.8** Torsion velocity of PZT beam versus ac current in conducting wire.

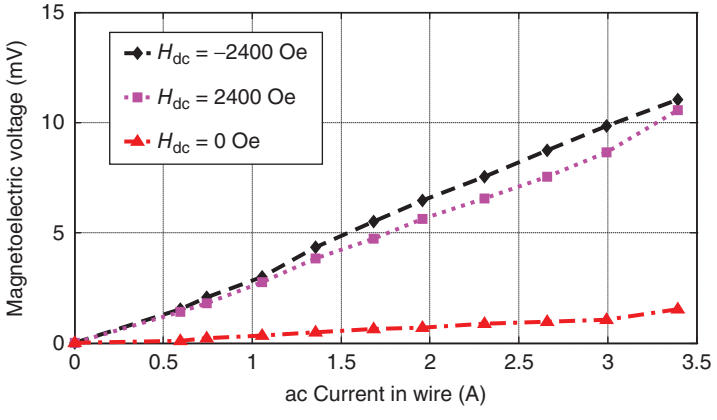


**Figure 1.9** ME voltage of PZT beam versus ac current in conducting wire.

velocity versus ac current amplitude were obtained. From the results, the conclusion that the ME response and torsion intensity could be controlled by adjusting the ac current in the conducting wire close to the beam was drawn. Therefore, the dc magnetic field actuating the beam with a linear response and high sensitivity would be achieved with the ac magnetic field applied perpendicularly to the plane of a piezoelectric beam.

The aforementioned experiments of the ME sensor and the magnetic actuator with piezoelectric ceramic have shown that the prototype of the ME sensor and the magnetic actuator without magnetic phase and also without applying power source was promising to be put into practical applications of magnetic field sensing and actuating technology.

## 1.4 Magnetoelectric Effect in Insulating Polymers

With the advent of science and technology, the performance of the insulating polymers attracted great attention from the researchers. However, little research

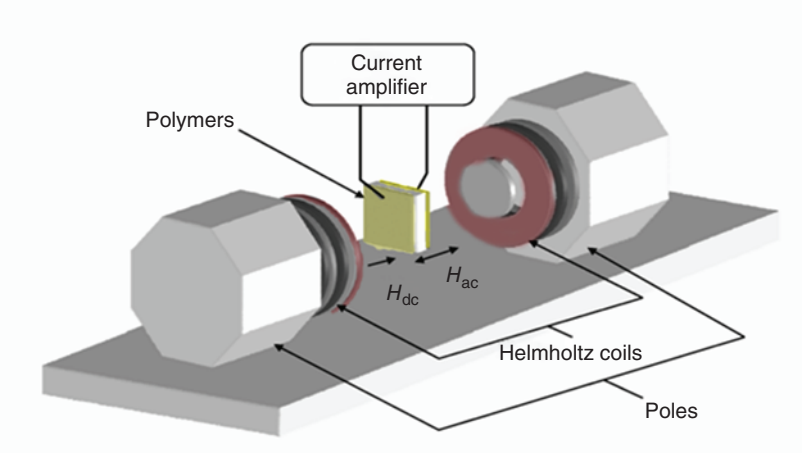


**Figure 1.10** ME measurement system [16].

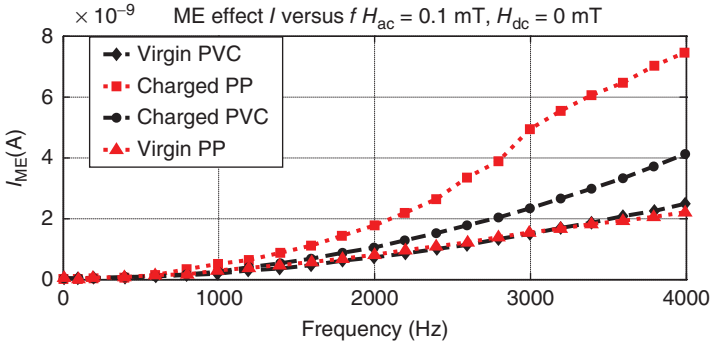


**Figure 1.11** Comparison of ME current between discharged and nondischarged porous PP.

work has been done on the comparison of the charge-storage ability among the different electrets by using the ME measuring system. In order to investigate the ME performances before and after high-voltage corona treatment of different electrets, the discharged porous polypropylene (PP) and polyvinyl chloride (PVC) had been chosen in the experiment.

As shown in Figure 1.10, because the ME current was induced by the integrated magnetic field, the suspended piezoelectric samples would be considered as the micro-generator whose ME effect could be suitably amplified by the current amplifier and the current subsequently observed by the oscilloscope.

As shown in Figure 1.11, the ME current in the corona-charged porous PP and PVC is higher than the nondischarged porous PP and PVC. Under the same poling conditions, the corona-charged porous PP possesses a higher ME current compared with the corona-discharged porous PVC.

This phenomenon is observed because the corona poling of the specimen led to the charge injection in the sample surface and volume and then formed a space-charge layer, which augmented the capacitance of the charged films due to

the interfacial polarization after corona poling. It is indicated that the porous PP, which possesses better charge-storage ability, can enhance ME effect response. And the charges injected in the polymers can have an effect on the ME effect responses.

The basic element model can be established as follows: the induced eddy currents originate from the applied magnetic field, which induces magnetic flux through the surface measurement of the electrodes $S$ and can be expressed as [15]

$$\varphi = \iint_s B_{ac} \mathrm{d}S \tag{1.1}$$

where $B_{ac}$ is ac magnetic induction vector. Consequently, electromotive forces (emfs: $V_{\text{Faraday}}$) appearing around loops in the metal electrode can be expressed as [17]

$$V_{\text{Faraday}} = -\mathrm{d}\varphi_{\text{loop}}/\mathrm{d}t = -\mathrm{d}B \cdot S/\mathrm{d}t = -j\omega B_{ac} \cdot S = -j\omega \cdot \varphi_{\text{loop}} \tag{1.2}$$

The equivalent circuit of the proposed modeling is as shown in Figure 1.12. In the schematic, the circuit with a capacitance $C_p$, a resistance $R_p$, and series with voltage source is equivalent to the sample in the magnetic field. The series with voltage source includes $V_{\text{Faraday}}$ and $V_{\text{ME}}$, which are from Faraday effect and ME effect, respectively. $R_c$ is the resistance measured with current amplifier.

The magnetically induced current $i_{\text{Lenz}}$ sources of the $V_{\text{Faraday}}$ in the circuit can be expressed as [17]

$$i_{\text{Lenz}} = v_{\text{Faraday}}/(Z + R_c) \tag{1.3}$$

Because $Z \gg R_c$, $i_{\text{Lenz}}$ can be expressed as [17]

$$i_{\text{Lenz}} = v_{\text{Faraday}}/Z \tag{1.4}$$

where $Z$ is the electrical impedance of the film at the measurement frequency and can be expressed as [17]

$$Z = R_p/(1/jC_p\omega) = R_p/(jC_pR_p\omega + 1) \tag{1.5}$$

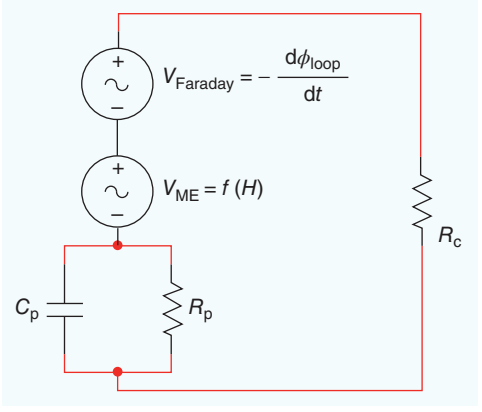


**Figure 1.12** Schematic of equivalent circuit. Zhang *et al*. 2014 [17]. Reproduced with permission of Elsevier.

Finally, resolving Eqs (1.2), (1.4), and (1.5) gives the calculated results of the Lenz current $I_{Lenz}$ as follows [17]:

$$I_{Lenz} = \omega \cdot \varphi_{loop}(C_p\omega - j/R_p) \tag{1.6}$$

The ME current $i_{ME}$ sources of the $V_{ME}$ in the circuit can be expressed as [17]

$$i_{ME} = V_{ME}/Z_c \tag{1.7}$$

where $V_{ME}$ is the ME alternative voltage and can be expressed as [17]

$$\begin{aligned} V_{ME} &= V_{ME}(H)|_{H=H_0} + \left.\frac{dV_{ME}(H)}{dH}\right|_{H=H_0} H + \frac{1}{2}\left.\frac{d^2V_{ME}(H)}{dH^2}\right|_{H=H_0} H^2 + \cdots \\ &= V_{ME}(H)|_{H=H_0} + e\times\left.\frac{dE_{ME}(H)}{dH}\right|_{H=H_0} H + \frac{1}{2}\times e\times\left.\frac{d^2E_{ME}(H)}{dH^2}\right|_{H=H_0} H^2 + \cdots \\ &= \text{Const} + e\times\alpha_E\cdot H + \frac{1}{2}\times e\times\beta_E\cdot H^2 + \cdots \end{aligned} \tag{1.8}$$

where $E_{ME}$ is the electric field, $e$ the thickness of the sample, $\alpha_E$ the ME voltage linear coefficient, and $\beta_E$ is second-order ME voltage coefficient. Because the voltage $V_{ME}$ is alternative root mean square (RMS) of the alternative value of ME voltage, Const = 0. And the ME current is a function of $H_{dc}$, which is a constant (in Figure 1.13), so $\beta_E = 0$.

The total current comes from both the magnetically induced current $i_{Lenz}$ and the ME current $i_{ME}$ [17]:

$$I_t = I_{ME} + I_{Lenz} \tag{1.9}$$

Finally, resolving Eqs (1.5), (1.7), and (1.8) gives the calculated results of the Lenz current $i_{ME}$ as follows [17]:

$$I_{ME} = V_{ME}/R_p(jC_pR_p\omega + 1) = V_{ME}(jC_p\omega + 1/R_p) \tag{1.10}$$

And the ME coefficient $\alpha_E$ is [17]

$$\alpha_E = |I_{ME}|/e\times H\sqrt{(C_p\omega)^2 + (1/R_p)^2} = |I_t - I_{Lenz}|/e\times H\sqrt{(C_p\omega)^2 + (1/R_p)^2} \tag{1.11}$$

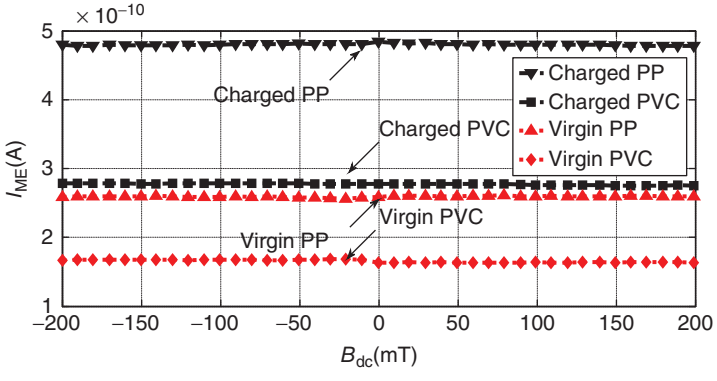


**Figure 1.13** Comparison of ME effect between charged and noncharged cellular PP and PVC (@Bac = 0.1 mT, $f$ = 1 kHz).

The investigation of ME performances in comparing the charge-storage ability among different electrets establishes the fact that enhanced ME performance could be achieved by using effective corona poling method on insulator polymers and not just by adding micro- or nano-additives into the specimen.

## 1.5 Conclusion

In this chapter, the ME effect and its application in single crystal, multilayered composites, and piezoelectric under Lorentz force induced by eddy current were discussed. A generalized ME effect was caused by an ac conducting wire and a piezoelectric beam from which a higher ME voltage coefficient was obtained than previous related research. The ME effects of such a designed piezoelectric beam set a good example of new ME systems without magnetic phase in the sample and also without applying power source on the piezoelectric beam. Magnetoelectric response of the magnetic actuator and the ME sensor composed of different electrets without magnetic phase is promising to be put into practical applications of magnetic field sensing and actuating technology.

## Acknowledgments

This work was supported by the Science and Technology Project of State Grid Corporation of China, National Natural Science Foundation of China (NSFC) (Grant No. 51307016), the State Key Laboratory of Engineering Dielectrics and Its Application (Ministry of Education, China), Opening Fund of Key Laboratory of Silicon Device Technology (Chinese Academy of Sciences), and Excellent Young Teachers Program of Northeast Dianli University. The authors would like to extend their sincere gratitude to Ms Feng Yan for her assistance in improving the English text.

## References

1 Lu, C., Xu, C., Wang, L., Gao, J., Gui, J., and Lin, C. (2014) Investigation of optimized end-bonding magnetoelectric heterostructure for sensitive magnetic field sensor. *Rev. Sci. Instrum.*, **85** (11), 115003.
2 Yu, X., Lou, G., Chen, H., Wen, C., and Lu, S. (2015) A slice-type magnetoelectric laminated current sensor. *IEEE Sens. J.*, **15** (10), 5839–5850.
3 Dong, S., Liu, J.M., Cheong, S.W., and Ren, Z. (2015) Multiferroic materials and magnetoelectric physics: symmetry, entanglement, excitation, and topology. *Adv. Phys.*, **64** (5-6), 519–626.
4 Leung, C.M., Zhang, S.Y., Or, S.W., Ho, S.L., and Lee, K.Y. (2012) *Proceedings of the 1st International Workshop on High-Speed and Intercity Railways*, Springer, Berlin, pp. 319–327.
5 Fiebig, M. (2005) Revival of the magnetoelectric effect. *ChemInform*, **36** (33), R123–R152.

6 Chen, L. and Qin, F. (2016) Enhanced sensitivity with a five-phase heterostructure magnetoelectric sensor at low magnetic bias field. *IEEE Trans. Magn.*, **52** (7), 2501304.

7 Nersessian, N., Or, S.W., and Carman, G.P. (2004) Magnetoelectric behavior of Terfenol-D composite and lead zirconate titanate ceramic laminates. *IEEE Trans. Magn.*, **40** (4), 2646–2648.

8 Guiffard, B., Guyomar, D., Garbuio, L., Belouadah, R., Zhang, J., and Cottinet, P.J. (2010) Eddy current induced magnetoelectricity in a piezoelectric unimorph bender. *Appl. Phys. Lett.*, **96** (4), 044105.

9 Leung, C.M., Or, S.W., Ho, S.L., and Lee, K.Y. (2014) Wireless condition monitoring of train traction systems using magnetoelectric passive current sensors. *IEEE Sens. J.*, **14** (12), 4305–4314.

10 Qiu, J., Chen, H., Wen, Y., and Li, P. (2015) Magnetoelectric and electromagnetic composite vibration energy harvester for wireless sensor networks. *J. Appl. Phys.*, **117** (17), 17A331.

11 Zhou, H.M. and Lian, J. (2014) A generalized lumped-element equivalent circuit for tunable magnetoelectric microwave devices with multi-magnetoelectric laminates. *J. Appl. Phys.*, **115** (19), 193908.

12 Tatarenko, A.S. and Bichurin, M.I. (2012) Electrically tunable resonator for microwave applications based on hexaferrite-piezoelectrc layered structure. *Am. J. Condens. Matter Phys.*, **2** (5), 135–139.

13 Tatarenko, A.S. and Bichurin, M.I. (2012) Microwave magnetoelectric devices. *Adv. Condens. Matter Phys.*, **10** (2012), 1–10.

14 Zhang, J.W. and Belouadah, R. (2014) Analysis on magnetoelectric effect induced by torsion moment in self-powered piezoelectric material. *Adv. Mater. Res.*, **1042**, 249–252.

15 Zhang, J.W. and Belouadah, R. (2014) A prototype of magnetic actuator based on generalized magnetoelectric phenomena: experiments and analysis. *Adv. Mater. Res.*, **1042**, 253–257.

16 Zhang, J.W. and Belouadah, R. (2014) Analysis on magnetoelectric responses of porous polypropylene and polyvinyl chloride after high-voltage corona discharge. *Adv. Mater. Res.*, **1042**, 70–74.

17 Zhang, J.W., Belouadah, R., Lebrun, L., and Guyomar, D. (2014) Magnetoelectric phenomena of insulator polymers after corona poling: procedure and experiments. *Sens. Actuators, A*, **220**, 112–117.